



Cite this: *New J. Chem.*, 2016, 40, 6796

# The synthesis and fast ethanol sensing properties of core-shell SnO<sub>2</sub>@ZnO composite nanospheres using carbon spheres as templates

Rui Zhang,<sup>a</sup> Tingting Zhou,<sup>a</sup> Lili Wang,<sup>\*a</sup> Zheng Lou,<sup>b</sup> Jianan Deng<sup>a</sup> and Tong Zhang<sup>\*ac</sup>

Core-shell SnO<sub>2</sub>@ZnO composite nanospheres were successfully prepared by using carbon spheres as sacrificial templates via a facile three-step procedure including a hydrothermal method. In contrast, pristine SnO<sub>2</sub> nanospheres and ZnO nanoparticles were obtained through a similar method with different steps, respectively. The composition and structures of the as-synthesized samples were confirmed by a series of characterization procedures. The obtained composite materials exhibited the special core-in-hollow-shell structure at the nanometer level. And as potential sensing materials, the obtained core-shell SnO<sub>2</sub>@ZnO composite nanomaterials demonstrated better gas sensing properties to ethanol including higher response, better selectivity, faster response and favorable repeatability, which may be related to the special core-in-hollow-shell structure with a porous surface and the hetero-contact between two different metal oxide semiconductors.

Received (in Montpellier, France)  
3rd February 2016,  
Accepted 31st May 2016

DOI: 10.1039/c6nj00365f

www.rsc.org/njc

## 1. Introduction

The emission of toxic gases and VOCs is extremely harmful to human life and health. Gas sensors have been used to detect the species and concentration of gases and have played a significant role in many aspects such as combustion process control, commercial production, human safety and environmental protection in recent years.<sup>1–3</sup> In order to manufacture gas sensors, considerable kinds of methods and materials have been applied. Because of their high surface energy, small size and high surface area-to-volume ratio, nanostructured materials have broadened the horizons of researchers and have been thought to be the promising materials for high-performance gas sensors.<sup>4,5</sup> Composite materials with complex structures such as core-shell structures have attracted a lot of attention because of their outstanding properties,<sup>6</sup> including a large fraction of the porous section exposed, little agglomerated configuration and high specific surface area. Recently, many studies on composite materials based on core-shell nanostructures have been reported. For example, Lou *et al.* have reported

the synthesis process of double-shelled SnO<sub>2</sub><sup>7</sup> and core-shell Fe<sub>2</sub>O<sub>3</sub>@SnO<sub>2</sub> cocoons,<sup>8</sup> which present an opportunity for people to achieve sophisticated functionalities, such as detection of gas species and concentration, by assembly of different selective shells and cores. Additionally, our group and that of Wang *et al.* reported core-shell Au@SnO<sub>2</sub> hollow nanospheres<sup>9</sup> with fast sensing performance to CO and core-hollow-shell α-Fe<sub>2</sub>O<sub>3</sub> nanospheres<sup>10</sup> as a sensing layer showing fast ethanol sensing properties. So, it is believable that sensing materials with the special core-shell nanostructure could offer enhanced gas sensing properties.

As chemically stable n-type semiconductors with the band gap of 3.6 eV and 3.37 eV,<sup>11,12</sup> ZnO and SnO<sub>2</sub> nanomaterials have been widely applied in gas sensors with various structures.<sup>13,14</sup> Zhang *et al.* reported porous SnO<sub>2</sub> hollow spheres exhibiting high response to ethanol.<sup>15</sup> Hu *et al.* reported ZnO sensing materials with multishelled hollow spheres displaying enhanced performance in gas sensing.<sup>16</sup> Although the sensors based on different structures of SnO<sub>2</sub> and ZnO nanomaterials have excellent sensing properties, reports of core-in-hollow-shell composite spheres with high-sensing performances are still rare. Therefore, an effective and facile synthetic strategy to develop multilevel nanostructures (core-in-hollow-shell spheres) is of great significance for gas sensors.

In this work, core-shell composite nanospheres and their single component have been synthesized. The synthesis of SnO<sub>2</sub>@ZnO core-shell composite nanospheres (CCNs) was achieved through a facile three-step method including a hydrothermal

<sup>a</sup> State Key Laboratory on Integrated Optoelectronics, College of Electronic Science and Engineering, Jilin University, Changchun, 130012, China.

E-mail: lili\_wang@jlu.edu.cn, zhangtong@jlu.edu.cn; Fax: +86 431 85168270;

Tel: +86 431 85168385

<sup>b</sup> State Key Laboratory for Superlattices and Microstructures, Institute of Semiconductors, Chinese Academy of Sciences, Beijing 100083, China

<sup>c</sup> State Key Laboratory of Transducer Technology, Chinese Academy of Sciences, Beijing 100083, China

procedure by using carbon spheres as sacrificial templates. In contrast to pristine SnO<sub>2</sub> nanospheres (NSs) and ZnO nanoparticles (NPs), the sensors based on SnO<sub>2</sub>@ZnO CCNs showed enhanced gas response to ethanol.

## 2. Experimental section

### 2.1. Chemical reagents

The starting materials were D-glucose (C<sub>6</sub>H<sub>12</sub>O<sub>6</sub>·6H<sub>2</sub>O), tin(II) chloride dihydrate (SnCl<sub>2</sub>·2H<sub>2</sub>O, 98%), absolute ethanol (CH<sub>3</sub>CH<sub>2</sub>OH, 99.8%), CTAB (C<sub>19</sub>H<sub>42</sub>BrN, 99%), zinc acetate dihydrate (Zn(Ac)<sub>2</sub>·2H<sub>2</sub>O, 99%) and distilled water. All starting chemicals used in this experiment were of analytical grade and were used as received without further purification.

### 2.2. Chemical synthesis

**Synthesis of SnO<sub>2</sub>@ZnO CCNs.** The synthesis of SnO<sub>2</sub>@ZnO CCNs was accomplished through a three-step chemical method according to literature reports.<sup>17–19</sup> However, experimental procedure and parameters were slightly modified in this work. Firstly, 0.5 M C<sub>6</sub>H<sub>12</sub>O<sub>6</sub>·6H<sub>2</sub>O was put into a 50 mL Teflon-lined stainless steel autoclave, which then was sealed and maintained for 5 h at 180 °C. The carbon spheres were obtained after centrifugation, filtration and drying. The second step was to achieve SnO<sub>2</sub> nanospheres that used carbon spheres as templates: 0.98 g of SnCl<sub>2</sub>·2H<sub>2</sub>O and 1 g of carbon spheres were dissolved in 60 mL of absolute ethanol under continuous ultrasonication for 1 h. The precursor was centrifuged, washed and dried after the carbon–Sn–ethanol mixture standing for 3 days at room temperature. Hollow SnO<sub>2</sub> NSs were obtained by annealing for 2 h at 600 °C (5 °C min<sup>-1</sup>) in a muffle furnace. The SnO<sub>2</sub>@ZnO CCNs were obtained through the third step: 0.34 g of Zn(Ac)<sub>2</sub>·2H<sub>2</sub>O and 0.7 g of SnO<sub>2</sub> NSs were added in the mixture of distilled water and ammonia under continuous stirring for 1 h at the temperature of 35 °C. In the meantime, 0.12 g of C<sub>19</sub>H<sub>42</sub>BrN was added into 10 mL of distilled water under the same conditions. Then the two solutions were mixed and stirred for another 2 h. The obtained suspension was transferred to a 50 mL Teflon-lined stainless steel autoclave and was heated for 16 h. The products were dried at 60 °C in a vacuum for 10 h after being obtained and washed with absolute ethanol and deionized water many times by filtration and centrifugation. Finally, the SnO<sub>2</sub>@ZnO CCNs were calcined for 3 h at 600 °C (5 °C min<sup>-1</sup>). In addition, SnO<sub>2</sub> NSs were synthesized without the third step and ZnO NPs were synthesized using only the third step without SnO<sub>2</sub> NSs for comparison.

### 2.3. Characterization techniques

The characterization (including composition and morphology) of products was done using different techniques. X-ray diffraction (XRD) patterns were recorded using a Scintag XDS-2000 X-ray diffractometer using Cu-Kα radiation (λ = 0.5418 nm) at a scan rate of 7° min<sup>-1</sup> in the range of 20–80° (2θ). Field emission scanning electron microscopy (FESEM) images were recorded on a JEOL 7500F microscope. Transmission electron microscopy

(TEM) and high-resolution transmission electron microscopy (HRTEM) along with selected area electron diffraction (SAED) were performed at 120 kV and 200 kV, respectively. The specific surface area was tested on a JW-BK132F analyser.

### 2.4. Fabrication and measurement of the SnO<sub>2</sub>@ZnO gas sensor

Typically, the primary fabrication process of the SnO<sub>2</sub>@ZnO side-heated gas sensor was described as follows:<sup>9,20</sup> the as-obtained powders were mixed with a few drops of deionized water and ground to form a homogeneous gas-sensing paste in an agate mortar using a grinding rod continuously. Then an alumina tube was covered with the paste using a brush, which was printed by two Au electrodes attached with a pair of platinum wires previously. In the following, a Ni–Cr alloy wire, as a heating source, was inserted into the alumina tube. It should be noticed that working temperatures (°C) of the sensor were calculated to be two times of the heating current (mA).<sup>21</sup> The gas-sensing data of SnO<sub>2</sub>@ZnO products were collected from a CGS-8 gas-sensing intelligent test system (Chemical Gas Sensor-8 Intelligent Gas Sensing Analysis System, Elite Tech, and Beijing, China). The typical schematic structure of a gas sensor and the theoretical diagram of the test circuit are shown in Fig. 1.

The resistance of metal oxide semiconductors changes in different gases due to the adsorption and reaction with molecules in air or tested gas. Hence, the response to different concentrations of tested gases was defined as follows: the resistances of the sensor in air and sample gas are  $R_a$  and  $R_g$ , respectively. And the response ( $S = R_a/R_g$ ) was the ratio of  $R_a$  to  $R_g$ . In addition, the response time ( $T_{r1}$ ) and recovery time ( $T_{r2}$ ) were measured as the time taken from  $R_a$  to  $R_a - (R_a - R_g) \times 90\%$  and  $R_g$  to  $R_g + (R_a - R_g) \times 90\%$  for a sensor at a certain temperature. Generally speaking, they were defined as the time required to change 90% resistance upon exposure to sample gas or ambient air.<sup>20</sup>

## 3. Results and discussion

### 3.1. Structural and morphological characteristics

The synthesis procedure of SnO<sub>2</sub>@ZnO CCNs is described in Scheme 1. The carbon spheres, as a sacrificial template, were first obtained by using hydrothermal method to endow the abundance of carboxy and hydroxyl groups (Scheme 1, step I).<sup>18</sup> The morphology and structures of the carbon sphere shown in Fig. 2a exhibit uniform-size particles with smooth surfaces.

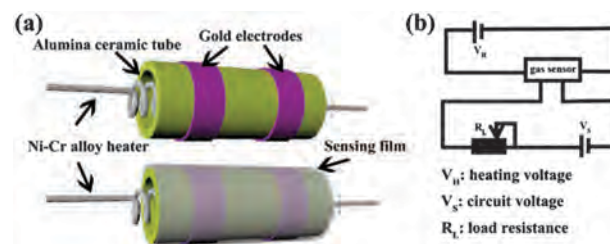
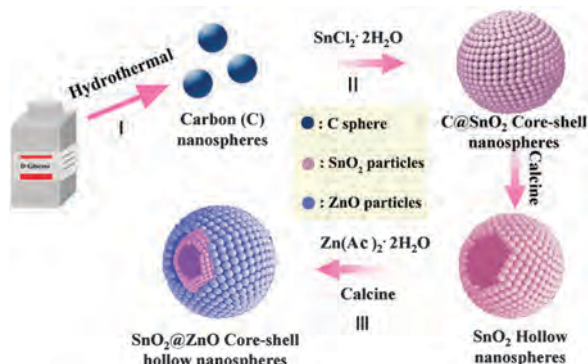


Fig. 1 Typical schematic structure of the gas sensor (a) and theoretical diagram of the test circuit (b).



**Scheme 1** Schematic illustrations of the synthesis procedure of SnO<sub>2</sub>@ZnO CCNs. (I) Hydrothermal fabrication of carbon spheres at 180 °C for 5 h; (II) fabrication of SnO<sub>2</sub> NSs using carbon spheres as templates and thermal annealing in air; (III) hydrothermal formation of SnO<sub>2</sub>@ZnO CCNs followed by calcination.

The introduction of positively charged Sn<sup>2+</sup> ions resulted in electrostatic interaction, which enabled self-assembly and self-adhesion between carbon spheres and Sn<sup>2+</sup> ions to form C@Sn-precursor core-shell nanospheres. With the increasing reaction time, the Sn-precursor further grew on the surface of carbon spheres caused by heterogeneous nucleation after saturation adsorption (Scheme 1, step II),<sup>22</sup> which made the rough surface of the C@Sn-precursor with the enlarged diameter of about 500 nm (Fig. 2b) compared with the carbon spheres (Fig. 2a). SnO<sub>2</sub> NSs were obtained using the calcination process to remove the carbon spheres. This procedure could result an oriented attachment aggregation of the neighbouring SnO<sub>2</sub> nanoparticles, resulting in nanoparticles being assembled together and close to each other (Fig. 2c). Finally, SnO<sub>2</sub>@ZnO CCNs were prepared through a hydrothermal method with the assistance of CTAB and subsequently calcination (Scheme 1, step III).

The significant effect of surfactants on the morphology of nanomaterials are well known and have been verified.<sup>23,24</sup> In aqueous solution, CTAB forms a large number of micelles. The hydrophilic parts facing the aqueous medium and lipophilic parts are associated with each other.<sup>25</sup> While a solution of 8.2 mM CTAB was obtained in this experiment, worm-like micelles were dominant instead of spherical micelles at a higher concentration of CTAB ( $C_{CTAB} > \text{critical micellar concentration (CMC)}$ ,  $\text{CMC} \approx 1 \text{ mM}$ ).<sup>24</sup> Under continuous mixing and hydrothermal conditions, SnO<sub>2</sub> NSs were used as the core and these worm-like micelles broke into short cylindrical micelles.<sup>26</sup> Then the Zn-precursors were gathered around the NSs-CTAB during the hydrothermal process. SnO<sub>2</sub>@ZnO CCNs were obtained with the outer diameter of about 250 nm using a calcination process, as shown in Fig. 2d. Interestingly, the as-obtained core-shell nanospheres had a loose core. The surface of spheres was porous and concave-convex, which consisted of nanoparticles. From the broken nanospheres (the red arrow), it could be seen that the nanocapsule possessed a distinctive core@void@shell configuration, which consisted of a rough core and a relatively thin shell. Moreover, FESEM images (Fig. 2e and f) vividly showed that the hollow shell had a typical porous structure.

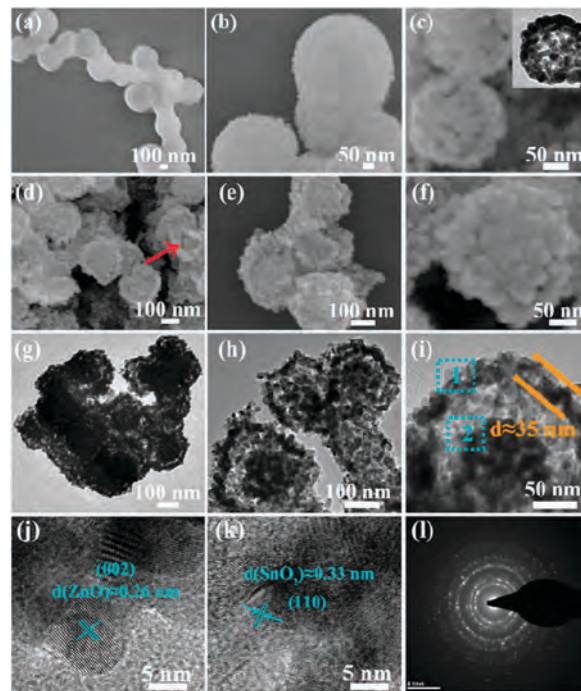


**Fig. 2** FESEM images of the as-synthesized samples: (a) carbon spheres; (b) C@Sn-precursor; (c) hollow SnO<sub>2</sub> spheres, the inset of (c) shows the corresponding image of TEM; (d–f) SnO<sub>2</sub>@ZnO CCNs, (g–i) TEM, (j and k) HRTEM and (l) SAED images of SnO<sub>2</sub>@ZnO CCNs.

More detailed interface structures and morphology of the SnO<sub>2</sub>@ZnO CCNs were further characterized using TEM and HRTEM. It could be observed that the shell ZnO nanomaterials were particle-like and completely covered the SnO<sub>2</sub> nuclei on the outside (Fig. 2g). And these nanospheres possessed distinct gaps between the shells and the cores (Fig. 2h). The average thickness of the shell of the sample was about 35 nm (Fig. 2i). The HRTEM images of the selected area (positions 1 and 2) in the inset of Fig. 2i showed the lattice planes of SnO<sub>2</sub>@ZnO CCNs. The lattice plane distance was 0.26 nm (Fig. 2j) and 0.33 nm (Fig. 2k), which corresponded to the (002) lattice plane of ZnO and the (110) lattice plane of SnO<sub>2</sub>, respectively. And the corresponding SAED pattern (Fig. 2l) presented ring-like, which confirmed that the SnO<sub>2</sub>@ZnO CCNs had polycrystalline structure.

For comparing and analysing the difference between the composite and pristine materials, the XRD patterns of the as-prepared single-component SnO<sub>2</sub> NSs (Fig. 3a) and ZnO NPs (Fig. 3b) revealed that all of the diffraction peaks could be precisely indexed to tetragonal rutile SnO<sub>2</sub> (JCPDS data card No. 41-1445) and hexagonal wurtzite ZnO (JCPDS data card No. 36-1451), respectively. After annealing for 2 h at 600 °C, the C@SnO<sub>2</sub> nanospheres were converted to loose and porous SnO<sub>2</sub> NSs (Fig. 3c) with the spherical-shape being retained. Fig. 3d shows the FESEM images of the as-synthesized ZnO NPs in the absence of SnO<sub>2</sub> NSs, which were composed of the nanoparticles with the diameter of about 40–60 nm.

The XRD patterns of SnO<sub>2</sub>@ZnO CCNs along with pure SnO<sub>2</sub> and ZnO from the standard data card are presented in Fig. 3e. Clearly, the pattern could be well indexed with the

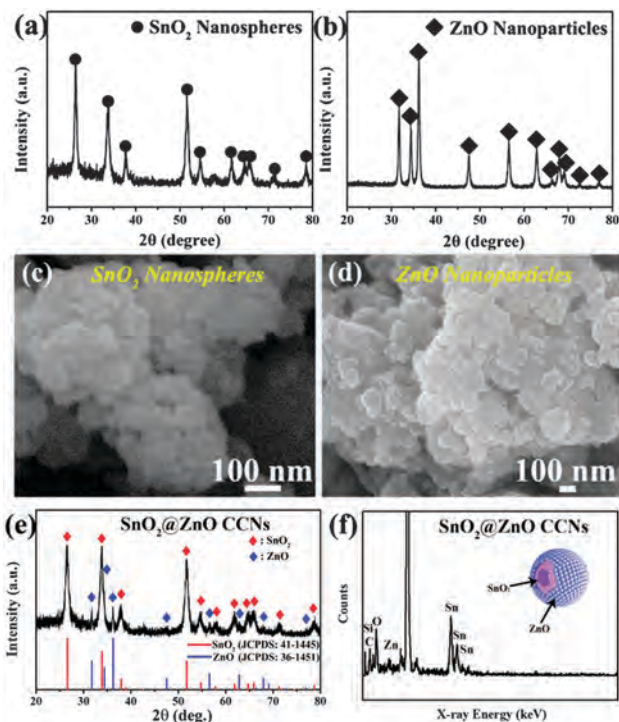


Fig. 3 The XRD patterns and FESEM images of SnO<sub>2</sub> NSs (a and c) and ZnO NPs (b and d). XRD spectra of the as-prepared SnO<sub>2</sub>@ZnO CCNs samples (e) and EDX pattern (f) of SnO<sub>2</sub>@ZnO CCNs.

characteristic diffraction peaks of hexagonal wurtzite ZnO (JCPDS data card No. 36-1451) and tetragonal rutile SnO<sub>2</sub> (JCPDS data card No. 41-1445). Moreover, there was no detection of other oxide peaks in the obtained diffraction peaks, and no obvious shift was observed, which revealed that carbon spheres were removed successfully after the calcination process. The elemental composition of the SnO<sub>2</sub>@ZnO CCNs was further confirmed by the EDX spectrum, which displays that the main components are Sn, Zn and O chemical elements (Fig. 3f). The Si peaks in the spectrum come from a SiO<sub>2</sub> substrate, which supported the sample before the measurements. The average atomic ratio of Sn and Zn is about 2.53:1 ( $At_{Sn}\% = 5.8$  and  $At_{Zn}\% = 2.29$ ). Based on the above XRD and EDX analyses results, the conclusion can be drawn that the as-obtained products are composed of SnO<sub>2</sub> and ZnO materials.

### 3.2. Sensing properties

Fig. 4a displays the sensing response depending on the working temperature for the detection of 50 ppm ethanol in air with three sensors based on SnO<sub>2</sub>@ZnO CCNs, SnO<sub>2</sub> NSs and ZnO NPs, respectively. The results revealed a general trend for metal-oxide semiconductor sensors, characterized by the maximum sensing response at a certain temperature. The maximum responses of three sensors based on SnO<sub>2</sub>@ZnO CCNs, SnO<sub>2</sub> NSs and ZnO NPs were 7.5, 3.5 and 4 to 50 ppm ethanol at 270 °C, 300 °C and 270 °C, respectively. It was obvious that SnO<sub>2</sub>@ZnO CCNs showed lower optimum working temperature and higher response compared with SnO<sub>2</sub> NSs and ZnO NPs.

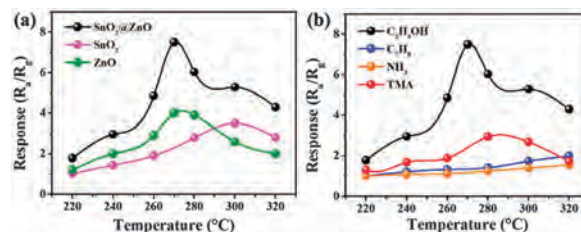


Fig. 4 (a) The relationship of the response and temperature of three sensors based on SnO<sub>2</sub>@ZnO CCNs, SnO<sub>2</sub> NSs and ZnO NPs sample to 50 ppm ethanol. (b) Response versus the different operating temperatures of the sensor based on composite materials exposed to 50 ppm C<sub>2</sub>H<sub>5</sub>OH, C<sub>3</sub>H<sub>9</sub>N, NH<sub>3</sub> and C<sub>7</sub>H<sub>8</sub>.

The high response of the SnO<sub>2</sub>@ZnO-based sensor to ethanol could be attributed to the special core-shell structure and the synergistic effect of two different n-type sensing materials. Therefore, an optimum working temperature of 270 °C was chosen for the SnO<sub>2</sub>@ZnO-based sensor in the following measurements.

It is known that different target gases have different optimum working temperatures.<sup>10</sup> Fig. 4b shows the selectivity of the gas sensor based on SnO<sub>2</sub>@ZnO CCNs towards 50 ppm of various tested gases at different working temperatures. It could clearly be seen that the sensor based on composite materials exhibited a higher response to ethanol (C<sub>2</sub>H<sub>5</sub>OH) than trimethylamine (C<sub>3</sub>H<sub>9</sub>N), ammonia (NH<sub>3</sub>) and toluene (C<sub>7</sub>H<sub>8</sub>). Thus, ethanol was selected to next evaluate the gas sensing performance of the sensor. Additionally, as shown in Fig. 4b, there was a steady increase before reaching the maximum response value of 7.5 at 270 °C for ethanol, and then the response gradually decreased with a further increasing temperature. In summary, the response was low at lower or higher temperature compared with the value measured at 270 °C, which was related to small chemical activation and the increase of adsorbed gas molecules escaping, respectively.<sup>27</sup>

Fig. 5a exhibits the dynamic response of the as-fabricated sensor based on SnO<sub>2</sub>@ZnO CCNs at 270 °C. It can be observed that the response of the sensor increased as the concentration of ethanol increased. In addition, the responses of the sensor to 10, 20, 50, 100 and 200 ppm ethanol were 2, 2.5, 7.5, 12.5 and 20, respectively. Response versus ethanol concentration characteristics of the sensors are shown in Fig. 5b. With the concentration of ethanol greater than 500 ppm, the growth

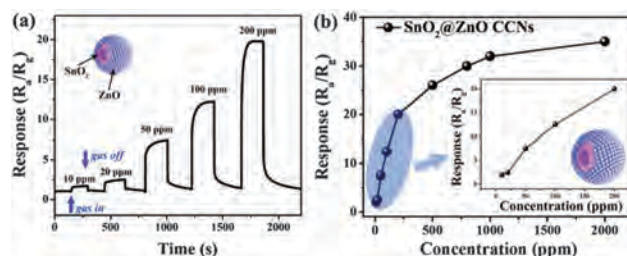


Fig. 5 (a) Transient response of the sensor to ethanol at the concentration of 10, 20, 50, 100, 200 ppm at 270 °C. (b) Responses of the sensor to 10–2000 ppm ethanol. Inset of (b) shows a partial enlargement response of the sensor to 10–200 ppm ethanol.

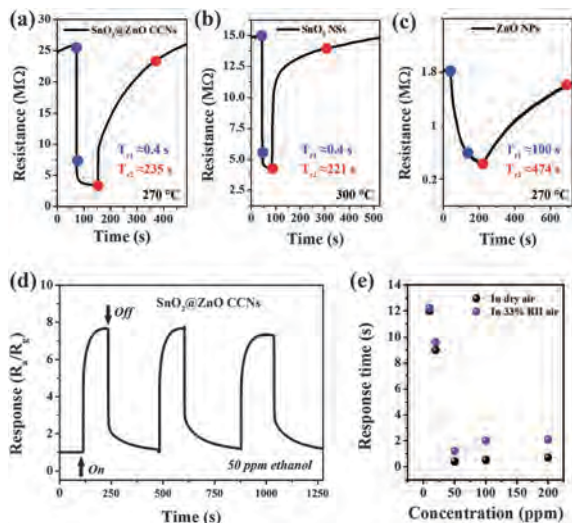


Fig. 6 Transient response curve of (a)  $\text{SnO}_2@ZnO$  CCNs; (b)  $\text{SnO}_2$  NSs and (c) ZnO NP-based sensors to 50 ppm ethanol. (d) Reproducibility of the sensor exposed to 50 ppm ethanol (3 cycles). (e) Response times of the sensor towards 10–200 ppm ethanol in dry air and wet air (33% RH).

rate of responses of the sensor becomes slower gradually. In particular, the  $\text{SnO}_2@ZnO$  CCN-based sensor revealed a high and fast growth rate of responses to ethanol in the range of 10–200 ppm (inset of Fig. 5b).

Besides, the response/recovery time of three sensors towards 50 ppm ethanol was investigated (Fig. 6a–c). Gas sensors based on hollow spheres ( $\text{SnO}_2@ZnO$ , Fig. 6a and  $\text{SnO}_2$ , Fig. 6b) show relatively fast response time compared to the sensor based on nanoparticles (Fig. 6c), which could be attributed to the special hollow structure with a porous surface. However, the recovery times of three structure-based sensors are relatively long in comparison to their response time values. It could be concluded that longer recovery times of gas sensors were observed because more oxygen molecules were re-adsorbed.<sup>28</sup> This process consists of the adsorption, dissociation, and ionization of oxygen on the surface.<sup>29,30</sup>

Keeping in mind the application value of the as-fabricated sensor, the reproducibility (Fig. 6d) of the sensor has also been tested. Three periods were tested at 50 ppm ethanol. After three periods, the sensor also retained the similar response to small variation. Fig. 6e demonstrates that the sensor showed a fast ethanol sensing response (<13 s) in dry air. Moreover, Table 1 shows the ethanol responses of  $\text{SnO}_2$ - or ZnO-based gas sensors reported from the literature.<sup>17,31–36</sup> A significantly improved property (response time to ethanol) was observed, which may play an important role in the real-time detection of ethanol.

Humidity is an important factor to be considered in real application for gas sensors. Thus, the effect of ambient humidity for the sensors was further studied. Then, the  $\text{SnO}_2@ZnO$ -based sensor was placed in an ambient atmosphere of 33% RH. The response time more or less increased (from 0.4 s in dry air to 1.2 s in 33% RH air towards 50 ppm ethanol).

Response to 50 ppm ethanol vs. relative humidity is shown in Fig. 7a. When RH < 40%, a slight variation occurred in the

Table 1 Comparison of  $\text{SnO}_2$ - or ZnO-based gas sensors towards ethanol reported before and in this work

Material	Structure	Tem./°C	Conc./ppm	Res.	$T_{r1}/T_{r2}/s$	Ref.
$\text{SnO}_2$	Hollow sphere	350	50	30	13/16	35
$\text{SnO}_2$	Nanosheet	350	100	48	8/–	32
ZnO	Hollow sphere	320	50	9.7	35/37.1	34
ZnO	Hollow sphere	300	300	275	36/35	33
ZnO/ $\text{SnO}_2$	Fibre	300	300	23	150/1100	31
ZnO/ $\text{SnO}_2$	Hollow sphere	200	100	380	74/12	17
ZnO/ $\text{SnO}_2$	Core-shell sphere	150	100	14.7	10/23	36
ZnO/ $\text{SnO}_2$	Core-shell sphere	270	50	7.5	0.4/235	This work

Tem.: temperature; Conc.: concentration; Res.: response ( $R_a/R_g$ );  $T_{r1}$ : response time;  $T_{r2}$ : recovery time; Ref.: reference.

sensing response. However, response approximately changed to half the value in high relative humidity of about 90%. The long term stability of the sensor in 50 ppm ethanol in 33% RH air or in dry air has also been investigated. In an ambient atmosphere of 33% RH air (Fig. 7b), the response of the sensor decreased from 7.5 to 7.0 in 12 days (decreased 6.7%). However, in dry air (Fig. 7c), the response decreased from 7.5 to 7.2 in 30 days (decreased 4.0%), and the maximum/minimum was 7.7/7.1, respectively. That is, humidity is a really negative factor for ethanol sensing in actual application.

It could be concluded that humidity has great influence on sensing response, which is a general feature of the metal oxide-based gas sensor.<sup>37,38</sup> The probable reason is explained in the following: (1) adsorption of oxygen and ethanol gases was blocked because of the introduction of water molecules, (2) water molecules react with the surface oxygen, resulting in a decrease in the sensor baseline resistance, and (3) as a weak acceptor, OH groups from  $\text{H}_2\text{O}$  may occupy adsorption sites, competing with the oxygen to react with ethanol.

### 3.3. Gas sensing mechanism of $\text{SnO}_2@ZnO$ CCNs

Compared with  $\text{SnO}_2$  NS and ZnO NP sensors, the  $\text{SnO}_2@ZnO$  CCNs showed enhanced sensing properties. The probable mechanism to ethanol was analysed as follows: firstly, the core-shell architecture made a contribution to the enhancement of ethanol sensing properties since many reports have indicated

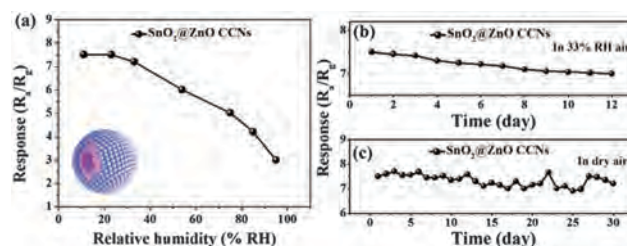
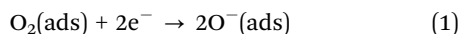


Fig. 7 (a) Relationship between the 50 ppm ethanol sensing response and relative humidity. (b) The responses (in 12 days) of the  $\text{SnO}_2@ZnO$  CCN-based sensor to 50 ppm ethanol in wet air (33% RH). (c) The responses (in one month) of the  $\text{SnO}_2@ZnO$  CCN-based sensor to 50 ppm ethanol in dry air.

that the morphology has great influence on the gas sensing properties.<sup>9,39</sup> Such a core-shell structure could protect the core from aggregation, which was an annoying problem for nanoparticles. In the meanwhile, the porous shell could offer good permeability for gas molecules and ions. Moreover, it was shown that the effective surface area had great influence on the gas sensing properties upon exposure to the target gas.<sup>40</sup> The SnO<sub>2</sub>@ZnO CCNs introduced in this work had a larger specific surface area (35.2 m<sup>2</sup> g<sup>-1</sup>) than SnO<sub>2</sub> NSs (13.8 m<sup>2</sup> g<sup>-1</sup>) and ZnO NPs (14.2 m<sup>2</sup> g<sup>-1</sup>). The increased surface area provided a better opportunity for the sensing materials to contact with gas molecules, which would benefit the diffusion of the tested gas (Fig. 8a).

Secondly, both SnO<sub>2</sub> and ZnO are n-type semiconductors, and the variation in resistance could be explained by the procedure of adsorption, oxidation and desorption. When the materials exposed to air, the oxygen molecules in ambient air were adsorbed on the surface of materials to form oxygen ions (O<sup>-</sup>), as a result of capturing the electrons from sensing materials, as follows:<sup>41</sup>



Thus the oxidation of the materials and the formation of the depletion layer, which appeared at the inner and outer of the surface, led to the increase of resistance of materials (Fig. 8c). In such core-shell SnO<sub>2</sub>@ZnO composite structures, electrons transfer from SnO<sub>2</sub> to ZnO at the interface until the Fermi levels equalize, while their work functions of them are 4.9 eV and 5.2 eV, respectively,<sup>42</sup> and the additional depletion layer is formed at the SnO<sub>2</sub> surface (Fig. 8b). Once the sensor is exposed to ethanol, the electrons are transferred from ethanol to the sensing materials and the depletion layers become narrowed. As a result, the conductivity of sensing materials (Fig. 7c) increased, which was described as follows:<sup>17</sup>

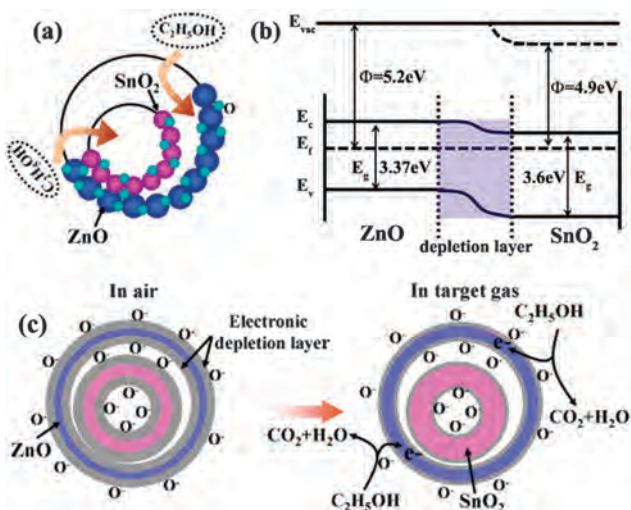
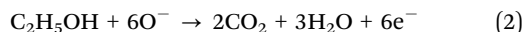


Fig. 8 Schematic diagram of sensing mechanism (a and c) and energy band structures (b) of the SnO<sub>2</sub>@ZnO CCN-based sensor.

Moreover, the synergetic effect of SnO<sub>2</sub> and ZnO made a positive contribution to the enhancement of the detection of ethanol.<sup>43,44</sup> These results revealed the considerable advantages of core-shell hollow nanospheres, which could be potentially useful in gas detection.

## 4. Conclusions

In summary, SnO<sub>2</sub>@ZnO CCNs were synthesized through a facile three-step method successfully using D-glucose, SnCl<sub>2</sub>·2H<sub>2</sub>O, absolute ethanol, CTAB, Zn(CH<sub>3</sub>COO)<sub>2</sub>·2H<sub>2</sub>O and ammonia as precursors. The composite material exhibits a special core-in-hollow-shell structure with an outer diameter of about 250 nm and a thickness of about 35 nm of the shell. Gas sensing results showed that the as-synthesized sensor exhibited enhanced ethanol sensing properties at the optimum operating temperature of 270 °C compared with SnO<sub>2</sub> NSs and ZnO NPs. The response to 50 ppm ethanol was up to 7.5, which is 2.1 and 1.9 times higher than that of SnO<sub>2</sub> NSs and ZnO NPs, respectively. In particular, the sensor exhibited a rapid response of as fast as 0.4 s. The rapid response could be ascribed to a synergetic effect between SnO<sub>2</sub> and ZnO along with the special core-in-hollow-shell structure with a porous surface, which could provide a sufficient active site. Thus, the excellent sensing activity of the composite nanosphere with a core-shell structure could make it one of the desirable candidates for applications in sensors.

## Acknowledgements

This research work was financially supported by the Postdoctoral Science Foundation of China (No. 2015M571361), the Natural Science Foundation Committee (NSFC, Grant No. 51502110 and 61504136) and the High Tech Project of Jilin Province (No. 20150204029GX).

## Notes and references

- J. H. Lee, *Sens. Actuators, B*, 2009, **140**, 319.
- Y. F. Bing, Y. Zeng, C. Liu, L. Qiao and W. T. Zheng, *Nanoscale*, 2015, **7**, 3276.
- S. Q. Tian, X. H. Ding, D. W. Zeng, J. J. Wu, S. P. Zhang and C. S. Xie, *RSC Adv.*, 2013, **3**, 11823.
- N. E. Barbri, A. Amari, M. Vinaixa, B. Bouchikhi, X. Correig and E. Llobet, *Sens. Actuators, B*, 2007, **128**, 235.
- H. R. Kim, K. I. Choi, K. M. Kim, I. D. Kim, G. Z. Cao and J. H. Lee, *Chem. Commun.*, 2010, **46**, 5061.
- S. F. Si, C. H. Li, X. Wang, Q. Peng and Y. D. Li, *Sens. Actuators, B*, 2006, **119**, 52.
- X. W. Lou, C. M. Li and L. A. Archer, *Adv. Mater.*, 2009, **21**, 2536.
- X. W. Lou, C. L. Yuan and L. A. Archer, *Adv. Mater.*, 2007, **19**, 3328.
- L. L. Wang, H. M. Dou, Z. Lou and T. Zhang, *Nanoscale*, 2013, **5**, 2686.
- L. L. Wang, Z. Lou, J. N. Deng, R. Zhang and T. Zhang, *ACS Appl. Mater. Interfaces*, 2015, **7**, 13098.

- 11 L. Z. Yu, L. C. Zhang, H. J. Song, X. M. Jiang and Y. Lv, *CrystEngComm*, 2014, **16**, 3331.
- 12 L. L. Wang, Z. Lou, T. Fei and T. Zhang, *J. Mater. Chem.*, 2011, **21**, 19331.
- 13 Y. E. Chang, D. Y. Youn, G. Ankonina, D. J. Yang, H. G. Kim, A. Rothschild and I. D. Kim, *Chem. Commun.*, 2009, 4109.
- 14 L. L. Wang, Z. Lou, T. Fei and T. Zhang, *J. Mater. Chem.*, 2012, **22**, 4767.
- 15 J. Zhang, X. H. Liu, S. H. Wu, M. J. Xu, X. Z. Guo and S. R. Wang, *J. Mater. Chem.*, 2010, **20**, 6453.
- 16 P. Hu, N. Han, X. Zhang, M. S. Yao, Y. B. Cao, A. H. Zuo, G. Yang and F. L. Yuan, *J. Mater. Chem.*, 2011, **21**, 14277.
- 17 W. Q. Li, Y. F. Li, G. J. Yang, Y. Z. Mao, J. Luo, D. J. Gengzang, X. L. Xu and S. H. Yan, *Sens. Actuators, B*, 2015, **211**, 392.
- 18 X. M. Sun and Y. D. Li, *Angew. Chem., Int. Ed.*, 2004, **43**, 597.
- 19 J. Zhang, S. R. Wang, Y. M. Wang, Y. Wang, B. L. Zhu, H. J. Xia, X. Z. Guo and S. M. Zhang, *Sens. Actuators, B*, 2009, **135**, 610.
- 20 L. L. Wang, T. Fei, Z. Lou and T. Zhang, *ACS Appl. Mater. Interfaces*, 2011, **3**, 4689.
- 21 T. Zhang, Q. Qi, K. X. Liu, L. Li, L. Zhang and B. K. Xu, *Trans. Nonferrous Met. Soc. China*, 2006, **16**, s780.
- 22 W. D. Shi, S. Y. Song and H. J. Zhang, *Chem. Soc. Rev.*, 2013, **42**, 5714.
- 23 T. Nguyen, D. Mrabet, T. Vu, C. Dinh and T. Do, *CrystEngComm*, 2011, **13**, 1450.
- 24 S. P. Wu, Z. L. Wang, X. Ouyang and Z. Q. Lin, *Nanoscale*, 2013, **5**, 12335.
- 25 L. S. Laurier, N. S. Elaine and G. M. D. Annu, *Annu. Rep. Prog. Chem., Sect. C: Phys. Chem.*, 2003, **99**, 3–48.
- 26 T. H. Ha, Y. J. Kim and S. H. Park, *Chem. Commun.*, 2010, **46**, 3164.
- 27 L. Liu, S. C. Li, J. Zhuang, L. Y. Wang, J. B. Zhang, H. Y. Li, Z. Liu, Y. Han, X. X. Jiang and P. Zhang, *Sens. Actuators, B*, 2011, **155**, 782.
- 28 B. Y. Kim, J. S. Cho, J. W. Yoon, C. W. Na, C. S. Lee, J. H. Ahn, Y. C. Kang and J. H. Lee, *Sens. Actuators, B*, 2016, **234**, 353.
- 29 K. I. Choi, H. R. Kim and J. H. Lee, *Sens. Actuators, B*, 2009, **138**, 497.
- 30 Y. H. Cho, X. Liang, Y. C. Kang and J. H. Lee, *Sens. Actuators, B*, 2015, **207**, 330.
- 31 E. Nikan, A. A. Khodadadi and Y. Mortazavi, *Sens. Actuators, B*, 2013, **184**, 196.
- 32 M. H. Xu, F. S. Cai, J. Yin, Z. H. Yuan and L. J. Bie, *Sens. Actuators, B*, 2010, **145**, 875.
- 33 L. Ge, X. Y. Jing, J. Wang, J. Wang, S. Jamil, Q. Liu, F. C. Liu and M. L. Zhang, *J. Mater. Chem.*, 2011, **21**, 10750.
- 34 X. S. Chen, X. Y. Jing, J. Wang, J. Y. Liu, D. L. Song and L. H. Liu, *CrystEngComm*, 2013, **15**, 7243.
- 35 J. Q. Xu, D. Wang, L. P. Qin, W. J. Yu and Q. Y. Pan, *Sens. Actuators, B*, 2009, **137**, 490.
- 36 X. C. Ma, H. Y. Song and C. S. Guan, *Sens. Actuators, B*, 2013, **188**, 193.
- 37 L. L. Wang, J. N. Deng, Z. Lou and T. Zhang, *J. Mater. Chem. A*, 2014, **2**, 10022.
- 38 D. X. Ju, H. Y. Xu, Z. W. Qiu, Z. C. Zhang, Q. Xu, J. Zhang, J. Q. Wang and B. Q. Cao, *ACS Appl. Mater. Interfaces*, 2015, **7**, 19163.
- 39 H. T. Fan, T. Zhang, X. J. Xu and N. Lv, *Sens. Actuators, B*, 2011, **153**, 83.
- 40 G. Lu, L. E. Ocola and J. H. Chen, *Adv. Mater.*, 2009, **21**, 2487.
- 41 S. S. Nath, M. Choudhury, D. Chakdar, G. Gope and R. K. Nath, *Sens. Actuators, B*, 2010, **148**, 353.
- 42 S. W. Choi, A. Katoch, G. J. Sun, J. H. Kim, S. H. Kim and S. S. Kim, *ACS Appl. Mater. Interfaces*, 2014, **6**, 8281.
- 43 B. Mondal, B. Basumatari, J. Das, C. Roychoudhury, H. Saha and N. Mukherjee, *Sens. Actuators, B*, 2014, **194**, 389.
- 44 E. Nikan, A. A. Khodadadi and Y. Mortazavi, *Sens. Actuators, B*, 2013, **184**, 196.